Austin Journal of Cardiovascular Disease & Atherosclerosis

Open Access

Austin Publishing Group

Research Article

Computational Simulation of Idealized Left Coronary Cardiac Structure with Bifurcation and Stenosis Topology

Jerin Tasnim Farin[1]; M Ferdows[1*]; KE Hoque[1,2]; Mohammad Zahidur Rahman Mazumder[3]

[1]Research Group of Fluid Flow Modeling and Simulation, Department of Applied Mathematics, University of Dhaka, Bangladesh

[2]Department of Arts and Sciences, Faculty of Engineering, Ahsanullah University of Science and Technology, Bangladesh

[3]Anesthesia, Analgesia and Intensive care, Cumilla Medical College and Hospital, Bangladesh

***Corresponding author: Mohammad Ferdows**
Research Group of Fluid Flow Modeling and Simulation, Department of Applied Mathematics, University of Dhaka, Dhaka, Bangladesh.
Email: ferdows@du.ac.bd

Received: January 09, 2024
Accepted: February 10, 2024
Published: February 17, 2024

Abstract

In this proposed study we are to investigate the variations in the geometry of the stenosis that exists at the bending regions in the left coronary artery with the basis of idealized 3D simulated artery models. Understanding the effects of plaque morphological characteristics such as the severity of stenosis, location, and eccentricity index is the main motive of this study. Atherosclerotic plaque severity is generally considered an indicator of cardiovascular diseases. However, the occurrence or probability of heart attack is not determined only by the stenosis severity. In fact, besides plaque severity, other local factors such as the location, bending regions, angle variations, and eccentricity of the plaques also play a vital role in such cases. Here, we have demonstrated the effects of stenosis based on its geometry and what impact it has on arterial flow patterns. We have shown the association of lesion eccentricity with other hemodynamic factors. The changes in the hemodynamic parameters have shed light on the conditions of left coronary artery stenosis at different locations of the artery, which is responsible for cardiovascular disease in human patients. To evaluate these effects, twelve computer-generated 3D artery models are considered. In these idealized models, we have considered three factors: bifurcation angle, stenosis degree, and eccentricity index of the plaque. Among the first seven are with a bifurcation angle of 60° degrees with one healthy model and eccentric and concentric stenosis of 25%, 50%, and 75% severity and the other seven are of 70° angular bifurcation with the same stenosis severity and geometry. Here, we have used open-source software for 3D model construction, mesh and grid generation, and hemodynamic simulations. From the resulting data we have analyzed significant changes in the behavior of arterial blood flow, for example, velocity profile, Fractional Flow Reserve (FFR), and Wall Shear Stress (WSS). Finally, these findings of variations in the stenosed bifurcated geometry will provide a more concise insight for a more specific assessment of those plaques that are vulnerable to cause coronary heart disease.

Keywords: LCA; CFD; Eccentricity Index (EI); Fractional Flow Reserve (FFR); Atherosclerosis; Wall Shear Stress (WSS)

Introduction

Coronary artery disease is the leading cause of mortality around the earth, and the illness's pathogenesis is still a mystery [1]. The interaction and complex correlation between blood flow dynamics, associated mechanical stress, and the remodeling of blood vessel properties has hampered detailed understanding of the formation and progression of atherosclerosis [2,3]. Despite recent breakthroughs in medical imaging procedures, determining complex biological dynamic behavior noninvasively and reliably remains a challenge. Computational fluid dynamics is an essential tool for focusing attention on modifications in flow dynamics in progression of the disease, and it has been used to evaluate how regulation of blood flow characteristics may presumably lead to formation and advancement of blood vessel-related diseases in the case of hemodynamics [4,5]. Indeed, employing high-resolution pictures gathered from innovative imaging modalities to perform CFD analysis on physiologically realistic simulation of blood flow remains a vital strategy for determining changes in biological variables related with coronary atherosclerosis [6-8]. The wall shear stress is a significant and potential factor of atherosclerosis severity. A

Citation: Farin JT, Ferdows M, Hoque KE, Mazumder MZR. Computational Simulation of Idealized Left Coronary Cardiac Structure with Bifurcation and Stenosis Topology. Austin J Cardiovasc Dis Atherosclerosis. 2024; 11(1): 1060.

healthy vascular physiology requires laminar shear stress, which is vital for protecting vascular diameter by managing cellular proliferation, thrombosis, and inflammation of the blood vessel walls [9]. As a result of the disruption in wall shear stress, blood vessel remodeling occurs, altering the physical behavior of the walls and, in the particular instance of arteriosclerosis, affecting plaque initiation and vulnerability. Atherosclerosis develops in regions of the carotid arteries where flow disturbances result in wall destabilization or extreme shear stress oscillations [10]. When the blood flow is steady and smooth, the blood vessels are affiliated in a horizontal path caused by mechanical influences exerted by the fluid on them. These cells would randomly place in the face of vibrational flow. Particle access and accumulation are frequently facilitated by the intercellular clefts that surround endothelial cells. Endothelial cells are more stretched in locations with low shear stress, according to in vivo research [11]. This indicates that locations with little shear stress are more likely to generate atherosclerotic plaques. On the other hand, as shear stress on endothelial cells reduces, fatty particle residence time in the circulation increases, as does the likelihood of penetration into the intima, hastening the formation of atherosclerotic plaque. The blood kinematic viscosity is one of the parameters that influences the calculation of pressure distribution and other hemodynamics. The non-Newtonian model has an effect on intra-cardiac blood flow as well [12]. Hemodynamic simulations with Newtonian and various non-Newtonian arterial viscosity models were used in the past literature [13-16]. However, little is known about how these models influence the outcomes of blood apparent viscosity, wall shear stress, pressure and velocity in biochemically realistic models of arteriosclerosis, and, more importantly, how accurate these models are at matching in-vivo measurements. One of the goals of this research is to see which blood viscous model can best reflect in-vivo blood flow dynamics measurements in patient-specific models with minor, moderate, and chronic atherosclerosis.

Significant atherosclerosis develops in the left coronary artery (LCA) particularly in the proximal Left Anterior Descending (LAD) and Left Circumflex segments (LCx). LCA is partitioned in such a way that it produces several complex geometries. Bifurcation LCA is a more common kind of coronary artery, accounting for 65.8% of the population [18]. Unsteady flow phenomena dominate blood flow in arteries. The cardiac system is a multibranch internal flow loop in which a complicated liquid circulates. The interaction between both the convective and viscous forces is governed by the Womersley number, a non-dimensional frequency parameter [17]. Arteries are living structures that can adhere to and change as hemodynamic conditions change. Unusual hemodynamic conditions can cause an aberrant biological reaction in some cases. The skewing of velocity profiles can result in pockets where the direction of wall shear stress fluctuates. Atherosclerotic disease is usually confined in these areas and resulting in a stenosis, or narrowing of the arterial lumen [19]. By causing turbulence and reducing flow through viscous pressure loss and flow choking, the stenosis can create turbulence and lower flow [20].

The severity of carotid stenosis is a regularly used indicator for determining stroke risk. The majority of people with extreme carotid artery disease, on the other hand, never have a massive heart attack, and strokes can happen even with mild - to - moderate stenosis [21]. This shows that factors other than the severity of stenosis at or around the vascular bifurcation may play a part in influencing stroke risk. Employing eccentrically and concentrically stenosed anthropomorphic carotid bifurcated models with comparable stenosis severity [22], we study the influence of stenosis architecture on fluid properties in the stenosed carotid bifurcation in this thesis. For severely and moderately stenosed instances, both computational models and flow rate visualizations differ significantly in flow patterns of eccentric and concentric stenosis models. We find that the size and location of the stenosis, as well as the geographic extent of enhanced wall shear stress, there are major differences between the two geometries of the stenoses. We recommend that the stenosed coronary artery bifurcation configuration the induced flow dynamics itself provide the most specific criteria for those atherosclerotic plaque that are vulnerable to increased thromboembolic potential and thus increased risk of developing cardiovascular disease, since these are also key physical and biological factors promoting thrombogenesis.

CAD is widely thought to be an inflammatory illness characterized by lipid accumulation in the artery wall as an early stage of atherosclerosis. Despite the fact that systemic susceptibility for atherosclerotic artery plaque formation, such as high cholesterol, diabetes, and hypertension, plaques form in localized locations in the coronary artery with dispersed flow and modest endothelial shear stress [23]. This study gives an overview of CFD techniques in CAD, covering kinematics and geometries of atherosclerotic lesions, plaque evolution, and rupture, as well as regional hemodynamics based on plaque position and composition. High shear loads around the stenosis can trigger platelets and cause thrombosis, which can completely shut down blood supply to the heart or brain [24]. The CFD allowed conventional and patient-based vascular models to simulate coronary blood flow conditions. The simulation enables non-invasive evaluation of hemodynamic parameters such blood movement magnitude, relative pressure differential, and FFR [25]. As a result, such hemodynamic mechanisms generate data on coronary constriction conditions and anticipate the degree of coronary arterial channel area, which would be the cause of patients' heart attacks. The expected effects in both circumstances have been reflected in the data, for example, an increased blood velocity inside the coronary veins tends to lengthen overall contrast agent gradient while a reduced blood velocity amplitude contributes to steepen the intravenous contrast gradient. The differential pressure and FFR data allow both unstenosed and stenosis artery models to be distinguished. All of these stats and observations are sufficient to warrant additional investigation in this area.

Methods

Reconstruction of Idealized Three-Dimensional Models of Left Coronary Artery

The majority of coronary major arteries are bifurcated almost everywhere. The majority of stenosis occurs near the branching or bending portions of the arteries. To describe these characteristics, we create an idealized model with variable Left Anterior Descending (LAD) and Left Circumflex (LCx) arteries that mimic patient-specific computed tomography coronary artery angiography. The 3D idealized models in this study are created using the computer-aided design software SolidWorks and then imported into the COMSOL Multiphysics version 6.0 software for grid generation and simulation. Because no digital scanning is available to load into COMSOL, the models are constructed to match views of the coronary artery junction during operations or imaging. The idealistic 3D model has two main arteries, the LAD and the LCx, each of which has one branch. The LAD is 9.5 cm long, whereas the LCx is 8 cm long. The models' structure

Table 1: Parameters for Grid independence.

Parameters	Extreme Coarse	Coarser	Coarse	Normal	Fine
Edge Elements	514	673	799	970	1214
Boundary Elements	4148	7396	9548	14638	21418
Total number of Elements	16695	37375	55171	104195	194533
Element Quality	0.6177	0.6681	0.678	0.6869	0.69
Maximum Element Size	0.0756 mm	0.0287 mm	.0227 mm	0.0151 mm	0.0151 mm
Minimum Element Size	0.0106 mm	0.00604 mm	0.00423 mm	0.00272 mm	0.0121 mm
Curvature Factor	1.0	0.8	0.7	0.6	0.5
Resolution	0.1	0.3	0.4	0.5	0.6

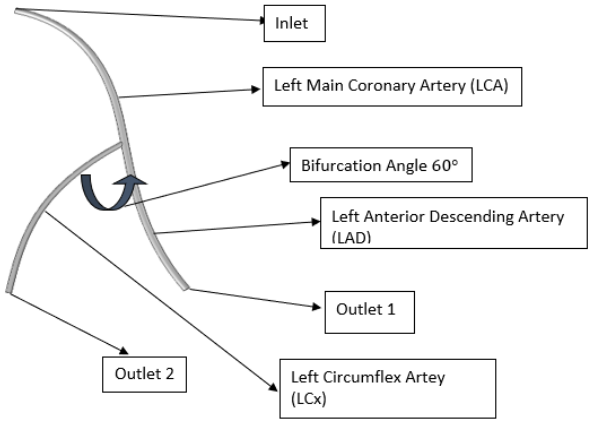

Figure 1: Left Coronary Artery (Healthy Model with 60-degree Bifurcation Angle.

and dimensions are based on a typical left coronary artery that matches anatomically close information. We utilize B-splines to bend the prototypes since they are straightforward to reflect the bending characteristics of the LAD, LCx, and side branches. We employ B-splines with the same origin but a different radius to construct the arterial tube. Using the difference in radii, we construct an artery wall that is solid on the inside to allow blood to flow freely. We can generate precise shapes of 3D idealized models using Boolean functions. The software is used to generate stenoses in the afflicted model. These computational models consist of one inlet and two outlets. The outlets have been represented as outlet 1 and outlet 2 respectively. The diameter of the inlet is 5mm and the diameters of the outlets are 4.6 mm and 3.8 mm each. We have constructed 14 computational 3D geometries. The first 7 models are constructed where we choose that the arterial bifurcation is 60°. The healthy (unstenosed) model and six diseased models are the total seven models. Among the diseased models, three types of stenosis have been chosen (mild 25%, moderate 50%, and severe 75% stenosis). Also in each stenosis model, two types of stenosis geometry are chosen (eccentric and concentric). We used SolidWorks software to calculate these angles. In the afflicted models the stenosis is placed shortly before the arterial bifurcation. It is preferable to save the model in STEP file format for use with the finite element model (FEM), which produces smooth perimeter walls with an inlet and two outlets in the areas of interest. Another set of seven models is developed by using arterial bifurcation at angle 70°. The other properties like stenosis geometry and severity of stenosis of these geometries are the same as the ones with angle 60°. The area of coronary stenosis (ACS) is calculated by the following equation:

$$\text{Percentage of stenosis} = \left[1 - \left(\frac{D_{stenosis}}{D_{normal}}\right)^2\right] \times 100\% \quad (1)$$

Here, $D_{stenosis}$ is the diameter of the artery at the stenosis region.

D_{normal} is the diameter of the artery's normal segment.

With these three-dimensional artery models, we proceed with our next steps. We import these models to the simulations software, generate mesh and grid, employ appropriate boundary conditions, and finally conducted the cardiac hemodynamics simulation.

Generation of Meshes and Grid Independency Test

We discussed the Finite Element analysis (FEM) that we employed in our research in this chapter. FEM is essentially a numerical approach for solving Partial Differential Equations (PDEs). The process begins with domain discretization, which divides the domain into cells, also known as elements, which form grids. Intricate configurations can be easily managed with this method because the grids are not required to be structured. An Arbitrary Eulerian Lagrangean (ALE) is projected to execute fluid flow and mesh displacement independently throughout the numerical simulation. We run a grid independency test after domain discretization to demonstrate convergence. Following that, a hemodynamic simulation is run with the proper boundary conditions. The discretization of the domain is the first stage in the finite element method. Finite elements are used to discretize the uneven domain into simpler and more regular subdomains. This is the same as substituting a system with a finite number of degrees of freedom for a domain with unlimited degrees of freedom. Various techniques can be used to simulate a domain by finite elements. Different ways of splitting the domain into finite elements take different amounts of time to compute and often result in different approximations of the physical problem solution. The discretization procedure is fundamentally a test of engineering judgment. Knowledge and experience of simple rules are required for efficient finite element idealization procedures.

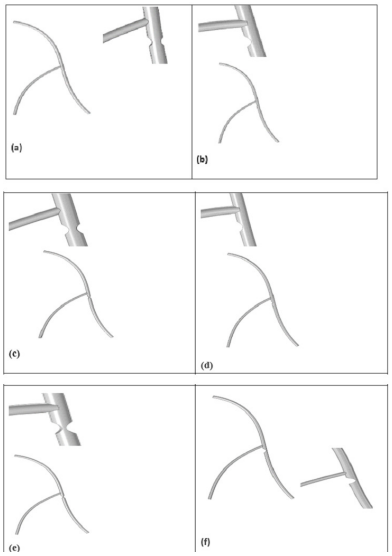

Figure 2: Different 60 degree stenosis models with different eccentricity and stenosis severity (a) 25% concentric model, (b) 25% eccentric model, (c) 50% concentric model (d) 50% eccentric model (e) 75% concentric model (f) 75% eccentric model.

After all of the models have been created, a mesh analysis is run to calculate the maximum and minimum mesh required for accurate results. The models are run for one periodic cardiac cycle at various mesh values until they reach the requisite convergence. In this scenario, our ideal 3D model has a non-uniform shape; finite element mesh production gives a concise and complete solution for curvatures and 3D volume cells. The surfaces and boundary areas of the nonlinear adapted triangle and tetrahedral cells are imported into the FEM simulation software. The mesh parameters used for fluid dynamics are COMSOL's predefined normal mesh size. Minor mesh settings changes are made to remove unnecessary elements and nodes and boost element densities all around the apex of the coronary artery bifurcation. The domain is adjusted to the normal setting that was previously defined. This choice resulted in a gradient in grid size, with smaller elements on the model's edges and bigger elements in the domain's center. Since the fluid velocity drops dramatically as it approaches the wall, the meshing gets finer as it gets closer to the boundary. Between both the border and the domain, the predefined meshes' fluid dynamic settings introduced a layer of elements. We employed tetrahedral elements in all of our models. In the three-dimensional computational domains of all LCA models, an isotropic mesh is built with settings such as a maximum output edge thickness of 1.5 mm for fine mesh. In the advanced settings, we also put boundary layers to the functional domain wall, as well as .463 mm edge elements and a layer diminishing ratio of 0.3. In the first diseased LCA model, there were 152081 meshes in total. The finer meshing results in higher-quality elements, which enhance numerical stability and raise the chances of obtaining a reliable solution. The total number of mesh elements in the domain is 194533, with 21514 in the fluid zone, 14638 in boundary elements, and 1214 in edge elements. The meshing's other parameters are the growth rate, which is set to 1.2, the curvature factor, which is set to 0.6, and the resolution in narrow regions, which is set to zero.

The enlarged views of the essential mesh portions such as the inlet, outlet, bifurcated portion, and the stenosis of the LCA model are shown in the following figure:

The grid independency test reveals how many components are needed in a model to verify that mesh size has no effect on the results of the analysis. After convergence to the desired precision, additional mesh refining has almost no effect on the results. The mesh no longer affects the model or its output. Only after a mesh independency analysis does a numerical discretization methodology like the Finite Element Method (FEM) converge to a solution. As a result, mesh independence is critical, and additional refinement isn't required once the required precision has been achieved.

For various mesh densities, a grid independency test for velocity profile has been performed. The mesh size ranges from extremely coarse to fine. In the following table (Table 1) we will show the parameters for different mesh size.

The finer meshing improves components, improves model correctness, and increases the likelihood of finding a feasible solution. The adaptable tetrahedral cells' interface and outer region are loaded into the FEM modeling application. Minor mesh settings modifications are done to remove extraneous elements and nodes while also improving element density in the stems of the blood vessel bending and stenosis. The meshings' other parameters are the boundary layer's growth rate, which is set to 1.5, the curvature factor, which is set to 0.6, as well as the resolution in confined regions, which is set to 0.5. We used extremely coarse, coarser, coarse, normal, and fine meshes, as well as the characteristics listed in Table 1, to test grid independency.

The grid independency for velocity magnitude indicates the accuracy of the numerical findings in the following graph when using these tabulated values in the finite element solver. Because the peak value amplitude of velocity in the computational

Table 2: Model parameters for different fluid models.

	Model	Effective Viscosity Equation	Parameters
1.	Newtonian [13]	$K = \mu_\infty$	$\mu_\infty = 0.0035\ Pa.s$
2.	Power law [13]	$K = m\dot{\gamma}^{n-1}$	$m = .0035\ Pa.s^n$, $n = 0.61$
3.	Carreau [13]	$K = (\mu_\infty + (\mu_0 - \mu_\infty)[1 + (\lambda\dot{\gamma})^2]^{\frac{n-1}{2}})$	$\mu_0 = 0.056\ Pa.s$, $\mu_\infty = 0.00345\ Pa.s$ $\lambda = 3.313\ s$, $n = 0.3568$
4.	Bingham-Papanastasiou [13]	$K = \mu_p + \frac{\tau_y}{\dot{\gamma}}\left[1 - e^{-(m_p\dot{\gamma})}\right]$	$\mu_p = .0146\ Pa.s$, $\tau_y = 0.0038\ N/m^2$, $m_p = 0.089\ s$
5.	Herschel-Bulkley-Papanastasiou [14]	$K = m\left(\frac{\dot{\gamma}}{\dot{\gamma}_{ref}}\right)^{n-1} + \frac{\tau_y}{\dot{\gamma}}\left[1 - e^{-(m_p\dot{\gamma})}\right]$	$m = 0.00521$, $n = 0.81$, $\tau_y = .0091\ Pa$, $\dot{\gamma}_{ref} = 226.5\ s^{-1}$, $m_p = .089s$
6.	Casson-Papanastasiou [14]	$K = \left(\sqrt{\mu_p} + \sqrt{\frac{\tau_y}{\dot{\gamma}}}\left[1 - e^{-(m_p\dot{\gamma})}\right]\right)^2$	$\mu_p = 0.0042\ Pa.s$, $\tau_y = .0038\ Pa$, $m_p = .089s$, $\dot{\gamma}_{ref} = 226.5\ s^{-1}$

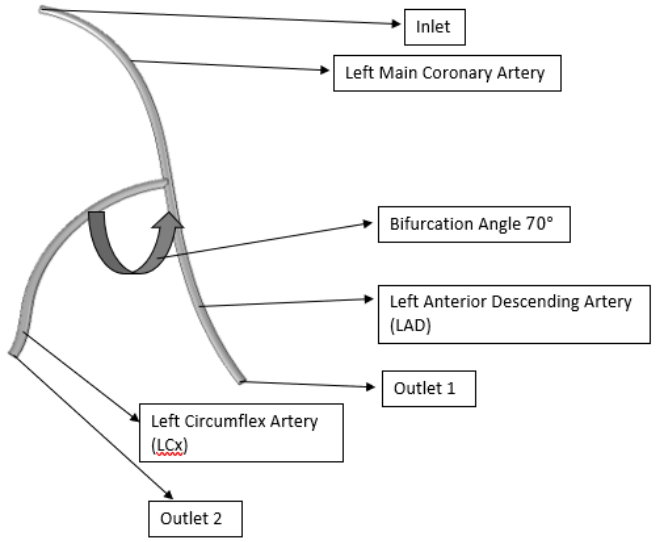

Figure 3: Left Coronary Artery (Healthy Model with 70-degree Bifurcation Angle.

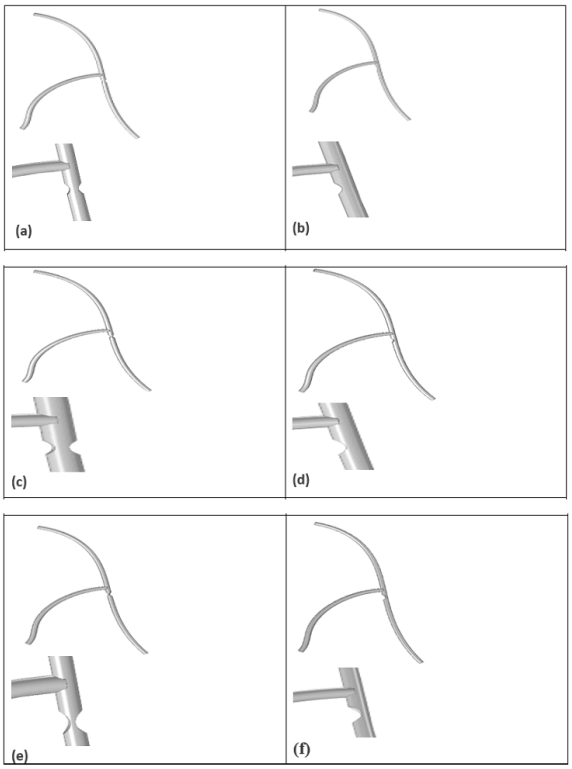

Figure 4: Different Stenosis models with different eccentricity and stenosis severity (a) 25% concentric model, (b) 25% eccentric model, (c) 50% concentric model (d) 50% eccentric model (e) 75% concentric model (f) 75% eccentric model.

domain is roughly identical for normal and fine meshes, we may deduce that the result is the same for finer and extremely fine meshes. As a result, the convergent finite element method used to describe the cardiac model. As a result, an element size of 72,273 was chosen to run all of the simulations in this investigation.

Here is the figure for grid independency test for pulsatile blood flow in five different densities of grids (Extremely coarse, coarser, coarse, normal, fine):

Boundary Conditions and Parameter Specifications

The flow rate of blood via an artery measured over time is known as the Arterial Input Function (AIF). The determination of AIF is required to quantify tissue perfusion. The AIF you choose can have a big impact on the blood flow maps you get from perfusion-weighted MR imaging. This method could be automated to eliminate operator dependency and improve consistency. The AIF plays a significant function in order to determine the concentration of fluid contrast agents in a time-independent condition at the coronary artery's outset point [17]. Perfusion parameters could be miscalculated if the AIF is calculated incorrectly.

The pre-processing begins by setting the time continuation parameter (t) to 0(s) and the relative velocity amplitude (alpha) to 1/3 globally. The following equation describes a piecewise function $f(t)$.

$$f(t) = \begin{cases} (1-\alpha)\sin(\pi t), & 0 \le t \le 0.50 \\ 1 - \alpha\cos\left(2\pi(t-0.5)\right), & 0.50 \le t \le 1.5 \end{cases} \quad (2)$$

This is a simple trigonometric piecewise function, where α is the relative pressure amplitude. During a cardiac cycle, pressure fluctuates between a minimum and a maximum value, which is determined using a relative amplitude. The first section of the function, between 0 and 0.50 s, seems to have no mechanical relevance; it is simply a ramp that allows the initial state to be calculated. During a 1 s cardiac cycle, the second half of the function causes the pressure to fluctuate between its lowest and highest values. The quantitative simulations are carried out for blood flows with stenosis areas ranging between 20% and 80%. The pressure and velocity measurements for the idealistic coronary artery model are determined by the computational results. The arterial input function is shown in the following figure:

Based on the finite element method, Comsol software has been used to analyze the inviscid Navier-Stokes equations as that of the governing equations of the flow of blood via stenosed arteries. The governing equations were discretized using the first-order upwind approach. Blood velocity was presumed to be single-phase, laminar, and unsteady in order to perform CFD simulations, and the Navier Stokes equations were formulated using these assumptions.

As mentioned, six rheological fluid models: 1) Newtonian, 2) Power Law, 3) Carreau, 4) Bingham-Papanastasiou, 5) Herschel Bulkley Papanastasiou, 6) Casson-Papanastasiou have been used to modeling considering blood viscosity. Table 1 includes the equations used in the fluid models and their parameters:

The simulation was developed by solving the three-dimensional Navier-Stokes equations for conservation of momentum and conservation of mass. These two equations are:

Mass Conservation Equation: $\rho\nabla . u = 0$ (3)

$$\rho\frac{\partial u}{\partial t} + \rho(u.\nabla)u = \nabla[-PI + K] + F \quad (4)$$ **Motion:**

Also, the corresponding Stokes equation is:

$$K = \mu[\nabla u + (\nabla u)^T] + \left(\frac{2}{3}\mu - \kappa\right)(\nabla . u)I \quad (5)$$

Where μ the dynamic viscosity of blood respectively, ∇u is is the velocity gradient vector and κ is the dilatational viscosity. For an incompressible fluid, the relation reduces to,

$$K = \mu[\nabla u + (\nabla u)^T] \quad (6)$$

Where u is the blood flow velocity, P is the pressure, K and ρ are the viscosity and density of blood respectively, ∇u is the velocity gradient vector, I is the identity vector.

A full hemodynamic examination of disrupted, spatial, and chronological flow dynamics may provide additional insight into

Table 3: Average Percentage difference of TA-velocity of the points at the center of the arteries between clinical measurements and CFD simulations for different models.

	Model	Percentage Difference (Mild Stenosis)	Percentage Difference (Moderate Stenosis)	Percentage Difference (Severe Stenosis)	Average Percentage Difference
1.	Newtonian	4.46%	5.1304%	7.51%	5.7%
2.	Power Law	20.62%	23.69%	34.713%	26.341%
3.	Carreau	1.81%	2.0869%	3.057%	2.318%
4.	Bingham-Papanastasiou	35.27%	40.52%	59.3631%	45.051%
5.	Casson-Papanastasiou	4.36%	5.013%	7.343%	5.572%
6.	Herschel-Bulkley-Papanastasiou	7.26%	8.347%	12.229%	9.278%

the progression of atherosclerosis and be of critical clinical importance. However, accurately assessing local flow patterns and mechanical stress in vivo is difficult. In this aspect, computational models are a useful tool. That is why, in patient-specific coronary models, precise boundary conditions are critical for obtaining high-quality physiological blood flow simulation [42]. Various types of BCs have been used by researchers, including analytical BCs, and explicit and implicit BCs. In the LCA models, explicit type boundary condition (Neumann type B.Cs) has been used. We assume that the cardiac pressure and circulation rate are periodical throughout time [17], with interval T, because the human heartbeat is almost periodic. The periodic cycle of the heart has been determined by the arterial input function mentioned above.

Accurate BCs are important for accurately capturing physiological blood flow patterns in vascular 3D models. The pulsatile blood circulation is replicated by pushing it into the artery's inlet [44]. For pulsatile flow characteristics, we used the inflow velocity profile in this investigation. This area of the influx cross - sections and the fluid velocity at the intake can both influence the amount of blood pushed in. Because the normal vector at the intake points outwards, the flow into the 3D patient vascular models is negative. As a result, the inflow condition becomes:

$$u(x, y, z, t) = u_{in}(t)$$

$$u = -U_0 \boldsymbol{n}$$

In the arterial domain, the specific inlet velocity waveform causes pulsatile behavior. The inlet velocity was set at 16.1* $f(t)$ cm/s. [17]

Because blood cannot circulate through the artery wall, it adheres to it due to its viscosity. As a result, on the walls of the models are set to rigid with no slip condition [30]. So, at the wall:

$$u = 0;\ v = 0;\ w = 0$$

Here, $n = (n_x, n_y, n_z)$ is the outward pointing normal to the outflow boundary.

The fluid is considered to be unidirectional at the outflow, and the pressure is proportional to the pressure just outside of the fluid [44]. The Pressure was set at 125* $f(t)$ mmHg [17]. Outflow Condition:

$$\frac{\partial u}{\partial n} = 0, \quad p = p_0$$

In a clinical investigation on arterial blood circulation, digital monitoring coronary angiography was applied to quantify the average blood velocity of the LAD, which was found to be 17.98 5.66 cm/s [31]. We compare the modeling results for angles 60 and 70 with the clinical evidence using a flow velocity measured in cm/s. The same method for materials, boundary conditions, and mesh generation are used to compute the flow velocity for the aortic bifurcation with angles 60 degree and 70 degree for different geometry and severity of stenoses.

Numerical Simulations

Navier-Stokes equations drove the flow hemodynamics calculations, which were performed using Comsol MultiPhysics on a Microsoft Windows 10 64-bit computer with 20 GB RAM and a core i-5 3.0 GHz CPU. The CFD analysis simulation was ran for 100-time steps at 0.01 s each time step, with each time interval representing one pulsatile myocardial flow for 1 s. The residual goals were set at less than 0.0001 in order to achieve a converged result, and the highest iteration number for each time step was 200. For post-processing, the results were saved in a "CFD post-compatible format". To investigate and examine the association between inclination angle, cardiovascular parameters, and atherosclerosis formation across distinct anatomical variations, Comsol fluid flow simulation was used to calculate flow streamline, flow velocity, WSS, and pressure gradient.

Finally, we explore numerous hemodynamic factors crucial to clinical outcomes using the finite element framework offered. More specifically, we focus on the relationship between these features and the flexibility of the vascular endothelium, as well as the importance of these characteristics to material properties. The WSS is useful in a wide range of situations. It's used to anticipate how atherosclerosis helps to form plaques. However, we study the impact of varying complexity in both geometries, including such Navier-Stokes and WSS arrangement of the artery wall. In addition, we examine the velocity profile in relation to stenosis severity, angulations, and eccentricity. The amplitude of the expansion and contraction is also described throughout the course of two cardiac cycles. In clinical examination, the amplitude of a blood artery after a stenotic area decreases significantly. The simulation results, which were obtained for actual system characteristics, are in qualitative descriptive agreement with the clinical data.

Numerical Simulations of Velocity Profile for different Arterial Geometry

In this study, we have considered fourteen different models of LCA structure. These models have been constructed by taking into considerations of stenosis severity, stenosis geometry and angular bifurcation. The changes in the velocity profile due to these characteristics are stated below:

a) Velocity contours of mild stenosis for 60 degree bifurcation angle:

b) Velocity contours of moderate stenosis for 60 degree bifurcation angle:

c) Velocity contours of severe stenosis for 60 degree bifurcation angle:

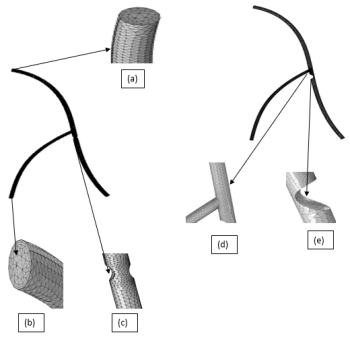

Figure 5: The tetrahedral grid generation: (a) outlet (b) inlet 1 (c) inlet 2 (d) stenosed region (e) bending region.

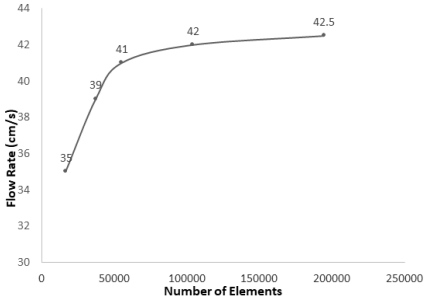

Figure 6: Grid independency Test.

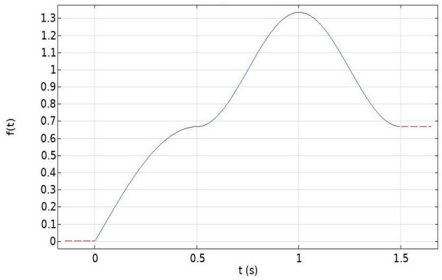

Figure 7: Arterial Input Function.

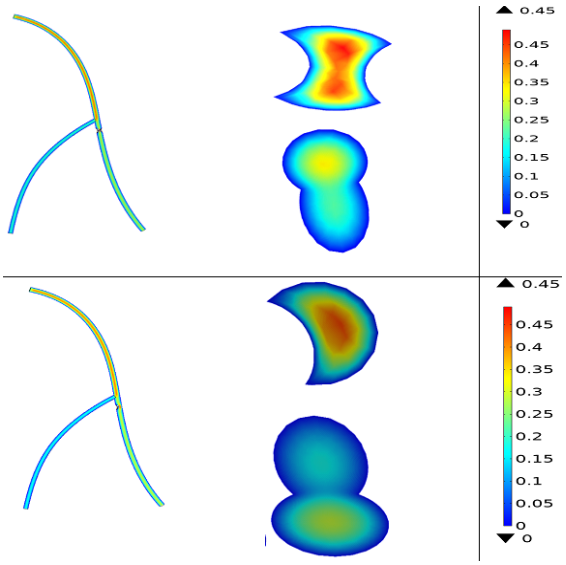

Figure 8: Velocity contours of 25% concentric stenosis for 60 degree angle.

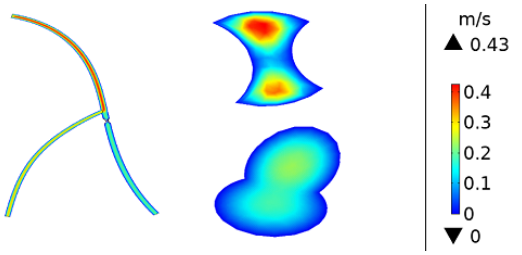

Figure 9: Velocity contours of 50% concentric stenosis for 60 degree angle.

d) Velocity contours of mild stenosis for 70 degree bifurcation angle:

e) Velocity contours of moderate stenosis for 70 degree bifurcation angle:

f) Velocity contours of severe stenosis for 70 degree bifurcation angle:

Numerical Simulations of Pressure Gradient

Numerical Simulations of Wall Shear Stress for different Arterial Geometry

Numerical Simulations of Different Rheological Models

We have considered six different rheological models for fluid flow simulations for healthy and diseased artery. We have observed a noticeable change in the hemodynamic parameters such as velocity pattern, pressure distribution and wall shear stress for the blood flow. Here, we are showcasing the cross-sectional views of the velocity gradients for those six blood flow models for arteries afflicted with mild stenosis. While simulating we have set the color range manually to 0 to 0.4 m/s. These are the maximum and minimum values respectively. Since the velocity amplitude ranges are fixed that's why, it is easy to compare how the velocity showcase differences in the simulation figures for different fluid models.

Result and Discussion

We give a comparison of many regular and pathological LCA models for modeling blood flow in this chapter. In the last chapter, we showed the results of our simulation. We'll talk about simulated data in this section. We estimated various hemodynamic variables (velocity profile, pressure differences and WSS). We additionally compared our data to literature [1] for validation purposes. In addition, we used line graphs and bar diagrams to demonstrate the comparisons so that the job could be understood more readily and correctly.

Validation of the Models

The discrepancies in Time Averaged (TA) velocity between clinical observations and CFD simulations of mild, moderate, and extreme stenosis models at the core of the arteries are shown in Figure 4:1. Experimental TA-velocity measurements are also presented as a bar diagram in this picture and compared to CFD findings calculated using several blood rheological models [13]. The magnitudes of the generated TA-velocities using CFD, as well as their percentage differences from clinical values, are also depicted in the image. The results of this figure show that blood viscosity models like the Power-law, Herschel-Bulkley-Papanastasiou and Bingham-Papanastasiou models yielded answers that were distinct from those of the other models. Table 4-1 displays the average % differences in TA-velocities (in the middle of the arteries) between clinical observations and CFD simulations for all stenosis models and tabulate the data seen in the figure. From the publication of Majid et al. we have extracted the clinical data. For 25%, 50% and 75% stenosis the flow velocity in the center of the artery is calculated as 0.2642, 0.23 and 0.157 [1]. Two non-Newtonian models – Carreau and Casson-Papanastasiou - have the least inconsistencies with clinical measurements, as indicated in the table. It's also worth noting that a model like Bingham-Papanastasiou has the potential to yield results that are as much as 50% different from clinical measurements.

Table 4: Pressure drop across the stenosis from proximal to distal main branch ΔP_{MB} fractional flow reserve in the main branch FFR_{MB} for all investigated cases:

Case	ΔP_{MB}(Pa)	FFR_{MB}
25% Concentric	38000	0.96
25% Eccentric	11000	0.98
50% Concentric	132000	0.82
50% Eccentric	17000	0.94
75% Concentric	335000	0.64
75% Eccentric	175000	0.799

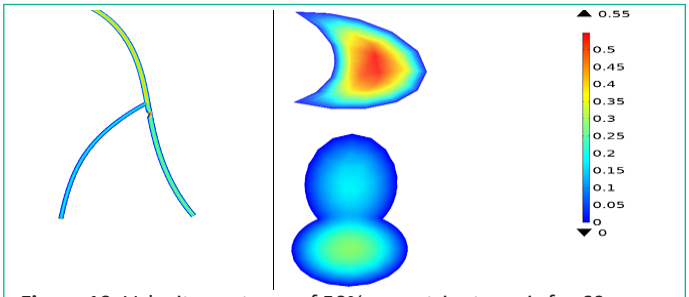

Figure 10: Velocity contours of 50% eccentric stenosis for 60 degree angle.

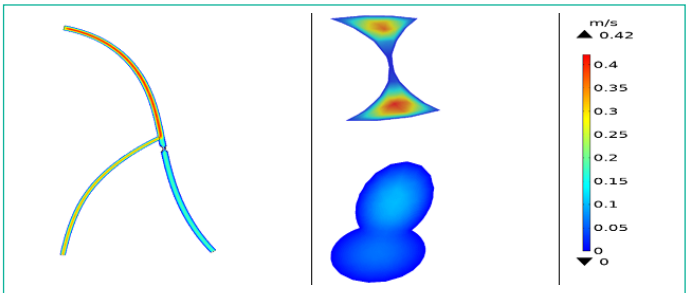

Figure 11: Velocity contours of 75% concentric stenosis for 60 degree angle.

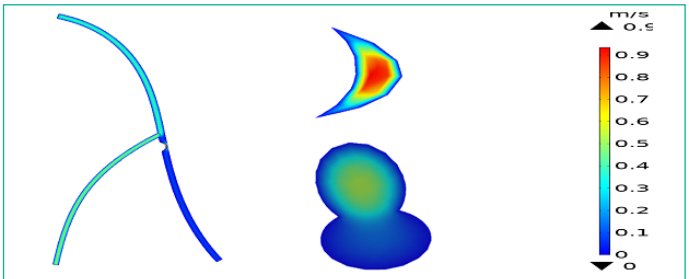

Figure 12: Velocity contours of 75% eccentric stenosis for 60 degree angle.

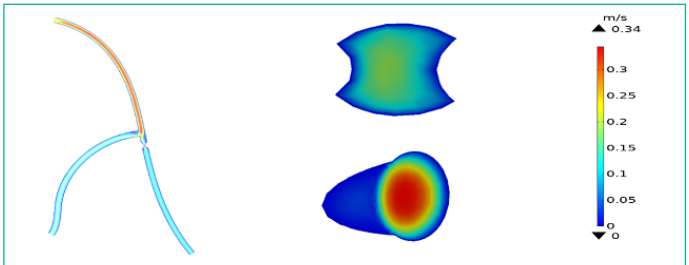

Figure 13: Velocity contours of 25% concentric stenosis for 70 degree angle.

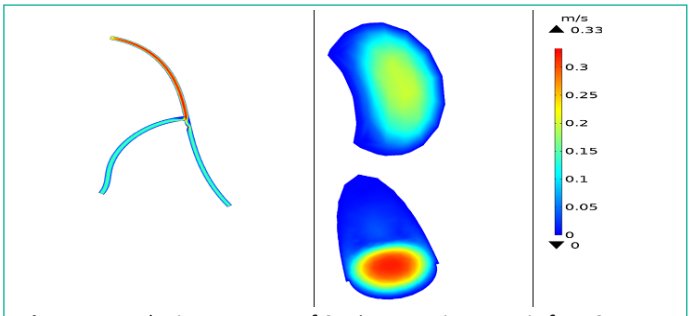

Figure 14: Velocity contours of 25% eccentric stenosis for 70 degree angle.

Velocity Pattern due to Severity of Stenosis

We have observed the velocity measurement at different regions of the stenosis (inlet, two outlets and stenosis regions). There are significant changes in velocity as the severity of stenosis keeps increasing. From the following bar diagram we observe that at the stenosis region the velocity is substantially very high. But the artery velocity witnessed a fluctuation (decrease) in the velocity just after passed through the stenosis region.

Velocity Pattern due to of Different Bifurcation Angle

Bifurcation angle has another important impact on the arterial velocity gradient. The velocity for greater bifurcation angle has about 16 percent increase in the velocity profile. On top of that due to changes in angle in the bending regions after the stenosis the blood flow drops magnificently in the arterial region which has greater bifurcation angle.

Velocity Pattern due to of Different Stenosis Geometry

Third important factor that has been considered in this study is the eccentricity of the stenosis. From the following observed data we conclude that concentric stenosis are more likely to showcase velocity fluctuations at the stenosis are. For concentric stenosis, the velocity starts with a higher velocity 40 cm/s and suddenly it drops down to 10 cm/s at the center and again peaks to 35 cm/s, whereas the eccentric stenosis also shows similar kind of behavior but the fluctuations rate is comparatively less that the concentric ones.

FFR Measurement

From the above table we have observed the pressure difference all along the LCA. From the FFR value we know that if the value is less than 1 then it means the atherosclerosis has started to begin. If it ranges between 0.75-0.80 then it is considered as borderline atherosclerosis. If we analyze the eccentric and concentric stenosis then we get to know that for the presence of concentric lesion the FFR value is likely to decrease abruptly. Although for the presence of acute eccentric stenosis the FFR value decreases, but it is still less than the concentric stenosis.

Observation of WSS for different Geometry of LCA

Wall shear stress is a very important factor to determine the plaque severity of stenosis at the LCA. The wall shear stress are mostly visible at the bifurcated regions and at the lesion of LCA. In the other regions of the LCA, the value of WSS.

Limitations

Although this thesis has drawn a correlation among several LCA attributes and favorable hemodynamic variables that are the major risk factors to develop atherosclerotic plaques, there are several drawbacks. In this study, we have assumed the artery walls as rigid and the motion of the artery muscle was not considered. Although previous studies have clearly demonstrated that wall velocity can be neglected in the unhealthy and stenosed arterial regions but considering it will help to acquire the desired result more correctly.

Conclusions

This study used Newtonian and five distinct non-Newtonian models to examine blood flow across 12 different ischemic LAD coronary arteries with low, medium, and acute eccentric and concentric stenosis. The Carreau and Casson-Papanastasiou viscosity flow models were shown to be adequate for calcu-

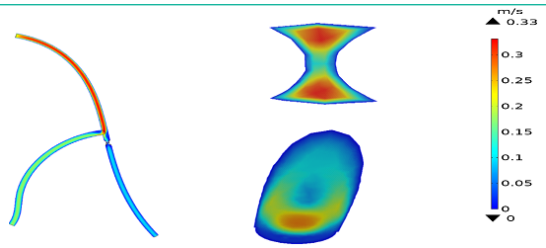

Figure 15: Velocity contours of 50% concentric stenosis for 70 degree angle.

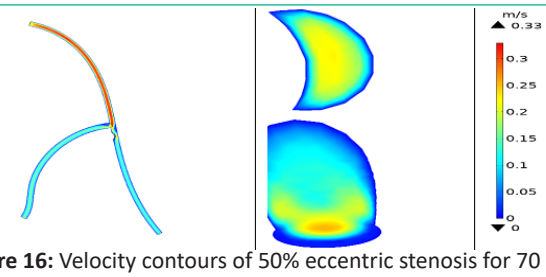

Figure 16: Velocity contours of 50% eccentric stenosis for 70 degree angle.

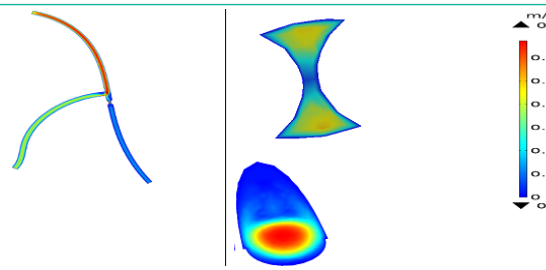

Figure 17: Velocity contours of 75% concentric stenosis for 70 degree angle.

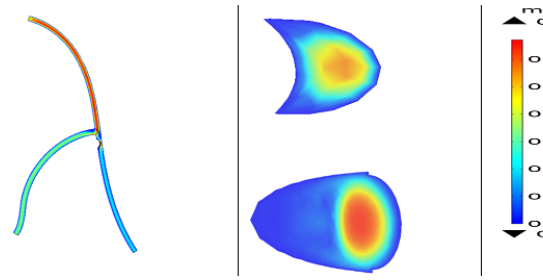

Figure 18: Velocity contours of 75% concentric stenosis for 70 degree angle.

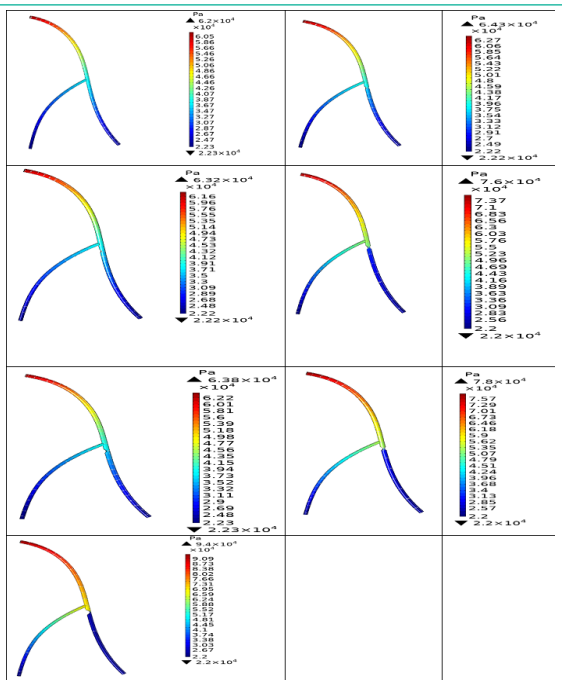

Figure 19: Pressure Gradient at the cross sectional region of stenosis.

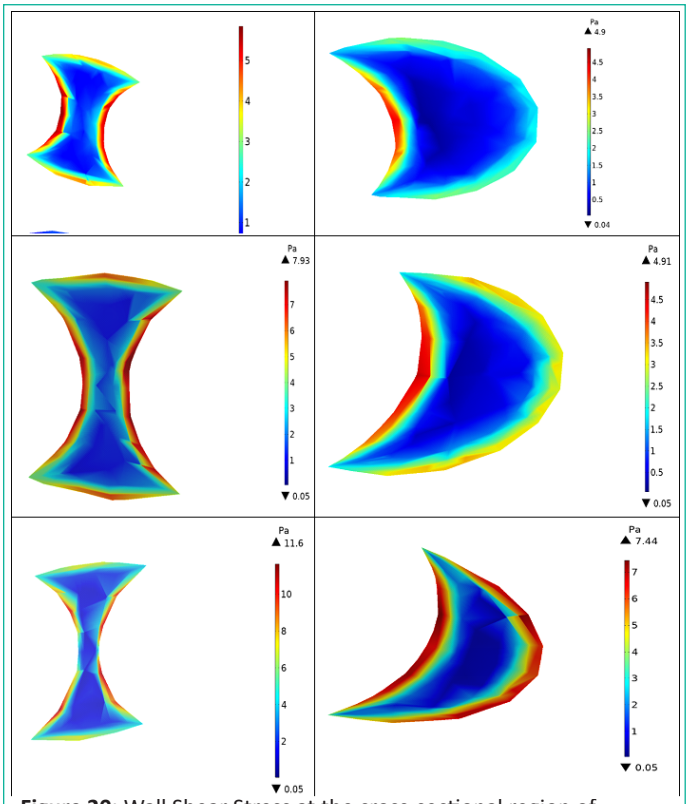

Figure 20: Wall Shear Stress at the cross-sectional region of stenosis.

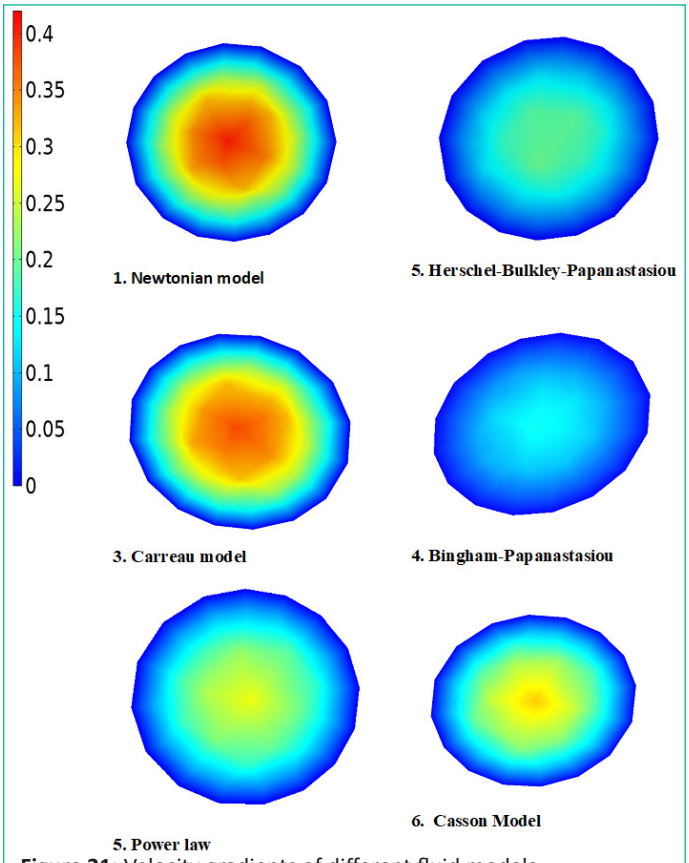

Figure 21: Velocity gradients of different fluid models.

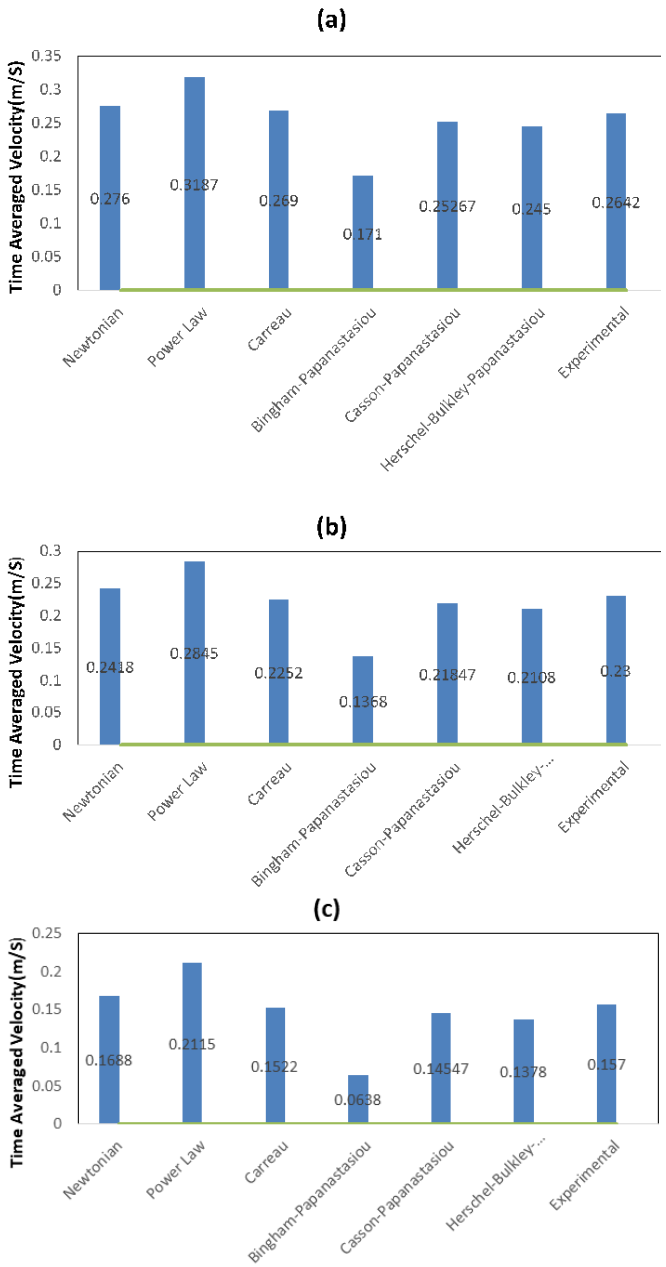

Figure 22: Comparison of TA velocity between clinical measurements and various rheological models for (a) mild stenosis, (b) moderate stenosis and (c) severe stenosis sizes.

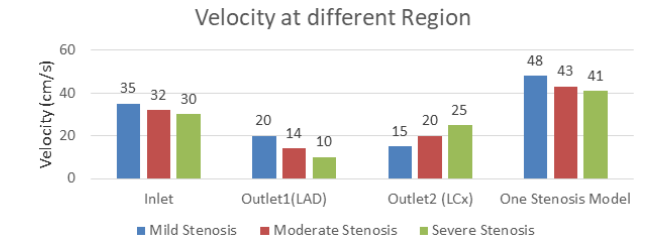

Figure 23: Velocity at different regions of different stenosis severity.

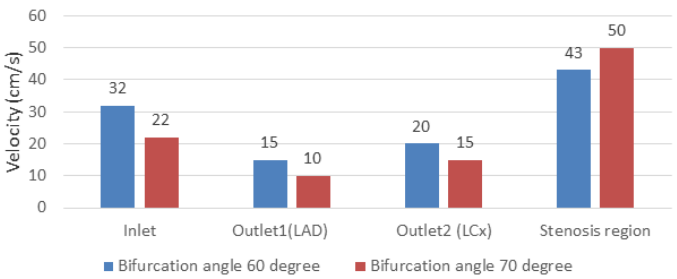

Figure 24: Velocity at different regions of different bifurcation angle.

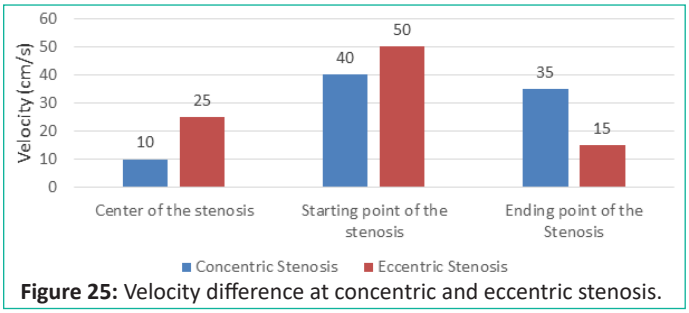

Figure 25: Velocity difference at concentric and eccentric stenosis.

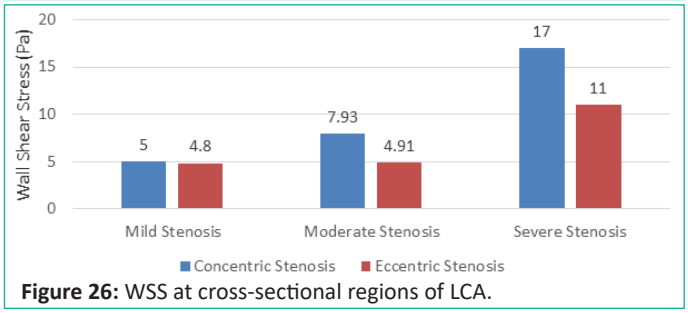

Figure 26: WSS at cross-sectional regions of LCA.

lating blood viscosity when velocities of single spots in the middle segment of the arteries were compared to numerical simulation results and clinical data. Blood flow can be regarded Newtonian fluid over the distal portion of the arteries and the sections with high WSS based on numerical simulations, which simplify the solution. However, this hypothesis is unacceptable in the proximal part and can have a major impact on simulation outcomes.

The hemodynamics of moderately and severely stenosed arterial bifurcations were studied in this study. In the bifurcated region, both concentric and eccentric stenosis models show dynamic and complicated flow patterns with asymmetric distribution of velocity, pressure and wall shear stresses. We discovered significant variations in these hemodynamic variables by changing stenosis geometry while preserving stenosis severity. Each model mild 25 percent, moderate 50 percent and severe 75 percent stenoses showed such disparities.

The general flow properties of equivalent 25 percent, 50 percent and 70 percent stenosed models are the same. The presence of a severe stenosis increases the size and extent of the recirculation zones, as well as introducing turbulence in the arterial region; this is in line with previous research. As a result, we may conclude that the significant changes in flow patterns found between both the eccentric and concentric stenosis models are certainly manifested at stenosis severity levels intermediate to those explored here.

Using an idealized coronary artery model, computational hemodynamics based on a numerical simulation environment was used to verify the influence of bifurcation angles of stenosis on coronary blood flow. The hemodynamic parameters are generated using a CFD solver (velocity magnitude, wall shear stress, pressure gradient). The following are our findings:

i. This study illustrates that blood flow is substantially higher in the stenosis region than in other parts of the 3D model due to the stenosis in the major LAD artery.

ii. The blood flow velocity passing through the stenosed region faces a marked fluctuations which is considered as one of the major symptoms of heart attacks.

iii. Although the velocity profile of eccentric and concentric stenosis does not differ much, but eccentricity has a greater impact while calculating the Fractional Flow Reserve (FFR).

Concentric stenosis is considered to be more risky as due to the presence of concentric stenosis, the FFR value falls down drastically.

iv. The impact of eccentricity on wall shear stress is proportional to the severity of stenosis. At mild stenosis level the wss does not differ much. But as the severity starts to increase from mild to acute, in concentric stenosis prone to become more dangerous than eccentric ones and show a higher wall shear stress in the lesion areas.

v. Among the six blood viscosity models we have used to check blood fluid characteristics, we conclude that Carreau and Casson-Papanastasiou models are mostly appropriate to describe the hemodynamics nature of blood as it aligns with the clinical data most closely.

We expect that the data generated in this study can be used in therapeutic settings, nevertheless, there are several limits to this process that will require additional research.

References

1. Asakura T, Karino T. Flow patterns and spatial distribution of atherosclerotic lesions in human coronary arteries. Circ Res. 1990; 66: 1045-66.
2. Nosovitsky VA, Ilegbusi OJ, Jiang J, Stone PH, Feldman CL. Effects of curvature and stenosis-like narrowing on wall shear stress in a coronary artery model with phasic flow. Comput Biomed Res. 1997; 30: 61-82.
3. Perktold K, Peter RO, Resch M, Langs G. Pulsatile non-Newtonian blood flow in three-dimensional carotid bifurcation models: a numerical study of flow phenomena under different bifurcation angles. J Biomed Eng. 1991; 13: 507-15.
4. Cheng S, Fletcher D, Hemley S, Stoodley M, Bilston L. Effects of fluid structure interaction in a three dimensional model of the spinal subarachnoid space. J Biomech. 2014; 47: 2826-30.
5. Cheng S, Jacobson E, Bilston LE. Models of the pulsatile hydrodynamics of cerebrospinal fluid flow in the normal and abnormal intracranial system. Comput Methods Biomech Biomed Engin. 2007; 10: 151-7.
6. Di Tomaso G, Pichardo-Almarza C, Agu O, Díaz-Zuccarini V. A multiscale and patient-specific computational framework of atherosclerosis formation and progression: a case study in the aorta and peripheral arteries. Procedia Comput Sci. 2015; 51: 1118-27.
7. Sakellarios AI, Bizopoulos P, Papafaklis MI, Athanasiou L, Exarchos T, Bourantas CV, et al. Natural history of carotid atherosclerosis in relation to the hemodynamic environment. Angiology. 2017; 68: 109-18.
8. Sakellarios AI, Papafaklis MI, Siogkas P, Athanasiou LS, Exarchos TP, Stefanou K, et al. Patient-specific computational modeling of subendothelial LDL accumulation in a stenosed right coronary artery: effect of hemodynamic and biological factors. Am J Physiol Heart Circ Physiol. 2013; 304: H1455-70.
9. Zhang B, Jin Y, Wang X, Zeng T, Wang L. Numerical simulation of transient blood flow through the left coronary artery with varying degrees of bifurcation angles. J Mech Med Biol 17.01. 2017; 17: 1750005.
10. Katritsis D, Kaiktsis L, Chaniotis A, Pantos J, Efstathopoulos EP, Marmarelis V. Wall shear stress: theoretical considerations and methods of measurement. Prog Cardiovasc Dis. 2007; 49: 307-29.
11. Olgaç U. Computational modeling of low-density lipoprotein transport in human coronary arteries: implications for atherosclerosis [diss.]. ETH Zürich. 2009.
12. Doost SN, Zhong L, Su B, Morsi YS. The numerical analysis of non-Newtonian blood flow in human patient-specific left ventricle. Comput Methods Programs Biomed. 2016; 127: 232-47.
13. Abbasian M, Shams M, Valizadeh Z, Moshfegh A, Javadzadegan A, Cheng S. Effects of different non-Newtonian models on unsteady blood flow hemodynamics in patient-specific arterial models with in-vivo validation. Comput Methods Programs Biomed. 2020; 186: 105185.
14. Cho YI, Kensey KR. Effects of the non-Newtonian viscosity of blood on flows in a diseased arterial vessel. Part 1: Steady flows. Biorheology. 1991; 28: 241-62.
15. Sochi T. 'Non-Newtonian rheology in blood circulation.' arXiv preprint arXiv:1306.2067; 2013.
16. Kumar D, Raviraj A, Vinoth R, Vijay Shankar CS. Non-Newtonian and Newtonian blood flow in human aorta: A transient analysis. Biomed Res. 2017.
17. Zaman N, Ferdows M, Xenos MA, Hoque KE, Tzirtzilakis E, et al. Effect of angle bifurcation and stenosis in coronary arteries: an idealized model study. Biomed Res. 2020; J4: 214-28.
18. Rabbi Md Foysal, Fahmida S Laboni, M Tarik Arafat. "Computational analysis of the coronary artery hemodynamics with different anatomical variations." Inform Med Unlocked. 2020; 19: 100314.
19. Ahmadpour-B M, Nooraeen A, Tafazzoli-Shadpour M, Taghizadeh H. Contribution of atherosclerotic plaque location and severity to the near-wall hemodynamics of the carotid bifurcation: an experimental study and FSI modeling. Biomech Model Mechanobiol. 2021; 20: 1069-85.
20. Tobias P, Curtiss LK. Thematic review series: the immune system and atherogenesis. Paying the price for pathogen protection: toll receptors in atherogenesis. J Lipid Res. 2005; 46: 404-11.
21. Steinman DA, Poepping TL, Tambasco M, Rankin RN, Holdsworth DW. Flow patterns at the stenosed carotid bifurcation: effect of concentric versus eccentric stenosis. Ann Biomed Eng. 2000; 28: 415-23.
22. Fakhim B, Javadzadegan A, Nakkas RT, Behnia M. Effect of stenosis eccentricity in a model of bifurcated coronary artery. Appl Mech Mater. 2014; 553: 332-7.
23. World Health Organization. World Health Rep. reducing risks, promoting healthy life. 2002.
24. Nadia A. On some mathematical models in hemorheology. Biotechnol Biotechnol Equip. 2014: 3286-91.
25. Wu J, Liu G, Huang W, Ghista DN, Wong KK. Transient blood flow in elastic coronary arteries with varying degrees of stenosis and dilatations: CFD modelling and parametric study. Comput Methods Biomech Biomed Engin. 2015; 18: 1835-45.
26. Niederer SA, Lumens J, Trayanova NA. Computational models in cardiology. Nat Rev Cardiol. 2019; 16: 100-11.
27. Weaver ME, Pantely GA, Bristow JD, Ladley HD. A quantitative study of the anatomy and distribution of coronary arteries in swine in comparison with other animals and man. Cardiovasc Res. 1986; 20: 907-17.
28. Bunton R, Jonas RA, Lang P, Rein AJ, Castaneda AR. Anomalous origin of left coronary artery from pulmonary artery: ligation versus establishment of a two coronary artery system. J Thorac Cardiovasc Surg. 1987; 93: 103-8.

29. Backer CL, Stout MJ, Zales VR, Muster AJ, Weigel TJ, Idriss FS, et al. Anomalous origin of the left coronary artery: a twenty-year review of surgical management. J Thorac Cardiovasc Surg. 1992; 103: 1049-1058.

30. Yau JM, Singh R, Halpern EJ, Fischman D. Anomalous origin of the left coronary artery from the pulmonary artery in adults: a comprehensive review of 151 adult cases and a new diagnosis in a 53-year-old woman. Clin Cardiol. 2011; 34: 204-10.

31. Ilia R, Rosenshtein G, Weinstein J, Cafri C, Abu-Ful A, Gueron M. Left anterior descending artery length in left and right coronary artery dominance. Coron Artery Dis. 2001; 12: 77-8.

32. Tarantini G, Migliore F, Cademartiri F, Fraccaro C, Iliceto S. Left anterior descending artery myocardial bridging: a clinical approach. J Am Coll Cardiol. 2016; 68: 2887-99.

33. Hongsakul K, Suwannanon R. Congenital absence of left circumflex artery detected by computed tomography coronary angiography: a case report. Case Rep Vasc Med. 2012; 2012: 204657.

34. Tousoulis D, Davies G, Kaski JC. A comparative study of eccentric and concentric coronary stenosis vasomotion in patients with Prinzmetal's variant angina and patients with stable angina pectoris. Clin Cardiol. 1998; 21: 643-8.

35. Chaichana T, Sun Z, Jewkes J. Haemodynamic analysis of the effect of different types of plaques in the left coronary artery. Comput Med Imaging Graph. 2013; 37: 197-206.

36. Weddell JC, Kwack J, Imoukhuede PI, Masud A. Hemodynamic analysis in an idealized artery tree: differences in wall shear stress between Newtonian and non-Newtonian blood models. PLOS ONE. 2015; 10: e0124575.

37. De Bruyne B, Sarma J. Fractional flow reserve: a review: invasive imaging. Heart. 2008; 94: 949-59.

38. Walburn FJ, Schneck DJ. A constitutive equation for whole human blood. Biorheology. 1976; 13: 201-10.

39. Karimi S, Dabagh M, Vasava P, Dadvar M, Dabir B, Jalali P. Effect of rheological models on the hemodynamics within human aorta: CFD study on CT image-based geometry. J Non Newtonian Fluid Mech. 2014; 207: 42-52.

40. Chiastra C, Iannaccone F, Grundeken MJ, Gijsen FJ, Segers P, De Beule M, et al. Coronary fractional flow reserve measurements of a stenosed side branch: a computational study investigating the influence of the bifurcation angle. Biomed Eng OnLine. 2016; 15: 91.

41. Kashyap V, Arora BB, Bhattacharjee S. A computational study of branch-wise curvature in idealized coronary artery bifurcations. Appl Eng Sci. 2020; 4: 100027.

42. Hoque KE, Ferdows M, Sawall S, Tzirtzilakis EE. The effect of hemodynamic parameters in patient-based coronary artery models with serial stenoses: normal and hypertension cases. Comput Methods Biomech Biomed Engin. 2020; 23: 467-75.

43. Hoque KE, Ferdows M, Sawall S, Tzirtzilakis EE, Xenos MA. The impact of hemodynamic factors in a coronary main artery to detect the atherosclerotic severity: single and multiple sequential stenosis cases. Phys Fluids. 2021; 33: 031903.

44. Choudhari P, Panse MS. Finite element modeling and simulation of arteries in the human arm to study the aortic pulse wave propagation. Procedia Comput Sci. 2016; 93: 721-7.